Journal of Geophysical Research: Solid Earth

RESEARCH ARTICLE
10.1002/2017JB015287

Effects of Melt Percolation on Zn Isotope Heterogeneity in the Mantle: Constraints From Peridotite Massifs in Ivrea-Verbano Zone, Italian Alps

Jian Huang[1], **Sha Chen**[1], **Xing-Chao Zhang**[1], **and Fang Huang**[1]

[1]CAS Key Laboratory of Crust-Mantle Materials and Environments, School of Earth and Space Sciences, University of Science and Technology of China, Hefei, China

Key Points:
- A first systematic study of Zn isotopic compositions for massif peridotites
- Low to moderate degrees of partial melting and sulfide melt percolation cause limited Zn isotopic variations in the mantle
- Silicate melt percolation induces large kinetic Zn isotope fractionation, a mechanism causing the Zn isotopic heterogeneity in the mantle

Supporting Information:
- Supporting Information S1

Correspondence to:
J. Huang and F. Huang,
jianhuang@ustc.edu.cn;
fhuang@ustc.edu.cn

Citation:
Huang, J., Chen, S., Zhang, X.-C., & Huang, F. (2018). Effects of melt percolation on Zn isotope heterogeneity in the mantle: Constraints from peridotite massifs in Ivrea-Verbano Zone, Italian Alps. *Journal of Geophysical Research: Solid Earth*, *123*, 2706–2722. https://doi.org/10.1002/2017JB015287

Received 29 NOV 2017
Accepted 16 MAR 2018
Accepted article online 24 MAR 2018
Published online 13 APR 2018

Abstract We determined Zn isotopic compositions of 21 orogenic peridotites from the Baldissero and Balmuccia peridotite massifs in Ivrea-Verbano Zone, Italian Alps, to investigate Zn isotope behaviors during partial melting and melt percolation in the mantle. The samples include lherzolites, harzburgites, and dunites. Lherzolites are strongly depleted in light rare earth element relative to middle and heavy rare earth element with $(La/Sm)_{PM}$ from 0.009 to 0.265 and $(La/Yb)_{PM}$ from 0.003 to 0.125, which can be explained by 5–15% fractional melting of a primitive mantle source. Harzburgites and dunites with nearly identical Mg# (molar 100 * Mg/(Mg + Fe) = 90.2–91.0) have $(La/Sm)_{PM}$ and $(La/Yb)_{PM}$ higher than but Zn contents similar to or lower than those of the parental lherzolites, suggesting that they were influenced by Zn-depleted silicate melt percolation. Lherzolites have δ^{66}Zn from 0.13 to 0.27‰ showing no correlations with indicators of melt extraction (e.g., Al_2O_3, Mg#, and La/Yb) and Zn contents. Three sulfide melt-affected lherzolites show similar δ^{66}Zn to the other normal ones. These observations indicate that 5–15% partial melting and sulfide melt percolation cause limited Zn isotope variations in the mantle. The metasomatic harzburgites and dunites display high δ^{66}Zn (up to 0.46‰) negatively correlated with Zn contents. Such correlations are attributed to kinetic effect during silicate melt percolation, whereby ^{64}Zn preferentially diffuses out from mantle minerals (e.g., olivine) to the percolating silicate melts. A diffusion model suggests that the negative correlation between δ^{66}Zn and Zn contents in dunites can be explained by an empirical β_{Zn} (i.e., β_{Zn}-exponent in $D_{66Zn}/D_{64Zn} = (m_{64Zn}/m_{66Zn})^{\beta Zn}$) of 0.05–0.06 in olivine.

1. Introduction

Zinc (Zn) is moderately volatile during planetary accretion and moderately incompatible during Earth's mantle melting. Zn and its isotopes have been widely used to trace a number of fundamental cosmochemical and geological processes including early solar system evolution, Moon formation, and crust-mantle interactions because of their volatile affinity and highly variable Zn isotopic compositions in meteorites and lunar and terrestrial materials (~18.0‰ δ^{66}Zn variations, e.g., Albarède, 2004; Moynier et al., 2017, and references therein). Mantle is the most important reservoir for Zn in the Earth (Palme & O'Neill, 2014) because the Earth's core contains negligible Zn due to its lithophile affinity during core-mantle differentiation (e.g., Li & Audétat, 2012; McDonough, 2014). Therefore, for better applications of Zn isotopes in mantle geochemistry, it is necessary to understand the behavior of Zn isotopes during partial melting and melt percolation in the mantle.

Doucet et al. (2016) found that refractory harzburgites with Al_2O_3 of 0.16–1.22 wt % from the Udachnaya kimberlite (Siberia) have lower δ^{66}Zn (0.14 ± 0.05‰, 2SD) relative to fertile peridotite xenoliths (Al_2O_3 = 3.73–4.76 wt %; δ^{66}Zn = 0.30 ± 0.03‰, 2SD) from Vitim (Siberia) and Tariat (Mongolia). They attributed such discrepancy to equilibrium Zn isotope fractionation during mantle melting. In contrast, Wang et al. (2017) recently showed that the unmetasomatic peridotites have a homogeneous δ^{66}Zn (0.18 ± 0.06‰, 2SD) regardless of their variable fertility (Al_2O_3 = 0.10–3.6 wt %), clearly indicating insignificant Zn isotope fractionation during mantle melting. However, in order to explain the slightly higher δ^{66}Zn of midocean ridge basalts (MORBs, 0.28 ± 0.03‰, 2SD), Wang et al. (2017) proposed that Zn isotopes can be fractionated by up to 0.10‰ during mantle melting. This is, however, inconsistent with the undistinguishable δ^{66}Zn (0.15–0.20‰) of komatiites and massif peridotites from the Southern Alps orogenic belt (Moynier et al., 2017). Consequently, the high δ^{66}Zn of MORBs is attributed to fractional crystallization of isotopically light olivine and/or Ti-Fe oxides (Chen et al., 2013; Moynier et al., 2017). These contradict on the interpretations of

δ^{66}Zn in peridotites, and mantle-derived lavas clearly highlight the importance to further investigate the Zn isotope behavior during mantle melting.

Crustal recycling and melt percolation are crucial for the chemical evolution of the mantle (e.g., Bodinier & Godard, 2014). Previous studies have shown that recycling of isotopically heavy subducted slab-derived components (e.g., carbonate melts and/or fluids) can dramatically modify the Zn isotopic composition of the upper mantle (Liu et al., 2016; Pons et al., 2016; Wang et al., 2017). However, the behavior of Zn isotopes during melt percolation has been not yet known, which significantly hampers the application of Zn isotopes to understand mantle geochemistry. Kinetic isotope fractionation induced by melt percolation has been observed for many isotope systems, such as Li, Mg, Ca, and Fe (Kang et al., 2017; Rudnick & Ionov, 2007; Weyer & Ionov, 2007; Zhao et al., 2017). Divalent Zn (Zn^{2+}, 0.74 Å) has similar ionic radius to Mg^{2+} (0.72 Å) and Fe^{2+} (0.78 Å) (Shannon, 1976) and thus substitutes for Fe and/or Mg in mantle minerals (Le Roux et al., 2010), implying that like Fe and Mg isotopes, Zn isotopes may be significantly fractionated during melt percolation in the mantle.

Zinc isotopic composition of the mantle can be deduced through studies of peridotite massifs tectonically exposed in the Earth's surface. Different to mantle xenoliths hosted by lavas, peridotite massifs allow an in situ observation of mantle processes and structural relationships between mantle lithologies (Bodinier & Godard, 2014). In addition, the isotopic composition of small-sized peridotite xenoliths could be modified by interaction with the host lavas during their entrainment and transport to the surface (such as Li and Mg isotopes, e.g., Ionov & Seitz, 2008; Pogge von Strandmann et al., 2011). To avoid such uncertainties, we here determined Zn isotopic compositions for a suite of well-characterized orogenic peridotites from the Baldissero (BD) and Balmuccia (BM) peridotite massifs (several km^2) in the Ivrea-Verbano Zone (Italian Southern Alps). Twenty-one peridotites studied here include lherzolites, harzburgites, and dunites. They are exceptionally fresh with no or limited modification (if any) by crustal materials and record variable degrees of partial melting and melt percolation in the mantle (Hartmann & Hans Wedepohl, 1993; Mazzucchelli et al., 2009, 2010; Shervais & Mukasa, 1991; Wang et al., 2013). The goal of this study is to examine the effects of partial melting and melt percolation on the Zn isotopic compositions of the mantle.

2. Geological Settings and Sample Descriptions

The Ivrea-Verbano Zone (Figure 1) in the Italian Southern Alps is one of the world's classic sections through the upper mantle and lower continental crust. In this zone, massif peridotites and granulite facies crustal rocks have attracted a lot of attention for several decades and can be used to constrain the composition and evolution of the upper mantle and lower continental crust (Mazzucchelli et al., 2010; Peressini et al., 2007; Wang et al., 2013, and references therein). The Ivrea-Verbano Zone was formed by the Alpine collision between the Adriatic and Europe Plates and consists of two main units of the Kinzigite Formation and the Mafic Complex (Shervais & Mukasa, 1991). The BD and BM peridotite massifs occur in the Mafic Complex along the western margin of the Ivrea-Verano Zone (Figure 1). They represent fragments of subcontinental lithosphere mantle tectonically emplaced at the lower crustal level, presumably in the Carboniferous or Permian (e.g., Peressini et al., 2007).

The BD (3×0.5–2 km^2) and BM (4.5×0.8 km^2) peridotite massifs mainly consist of spinel lherzolites with rare harzburgites (e.g., Mazzucchelli et al., 2010; Mukasa & Shervais, 1999; Obermiller, 1994; Shervais & Mukasa, 1991). Lherzolites from both massifs show similar average major and trace element compositions (Hartmann & Hans Wedepohl, 1993), and their chemical compositions record low to moderate degrees of melt extraction in the Paleozoic as revealed by the Paleozoic Re depletion ages (~370–500) and an Sm-Nd errorchron age (378 ± 48 Ma) of clinopyroxene separates (Mazzucchelli et al., 2010; Mukasa & Shervais, 1999; Obermiller, 1994; Rivalenti et al., 1995; Wang et al., 2013). Lherzolites are discordantly cut by two main generations of pyroxenite dykes that were subdivided into Cr-diopside suite and younger Al-augite suite based on both pyroxene chemistry and cross-cutting relationships (Mazzucchelli et al., 2010; Shervais & Mukasa, 1991; Wang & Becker, 2015a). These pyroxenite dykes reflect events of melt intrusion before the emplacement of the BD and BM peridotite massifs into the lower continental crust (Mukasa & Shervais, 1999; Wang & Becker, 2015a). Clinopyroxene trace element patterns suggest that Cr-diopside and Al-augite pyroxenites formed as cumulates from deep-seated melts of similar compositions with the latter representing more evolved products (Rivalenti et al., 1995). Two types of pyroxenites have Sr-Nd-Os isotopic ratios

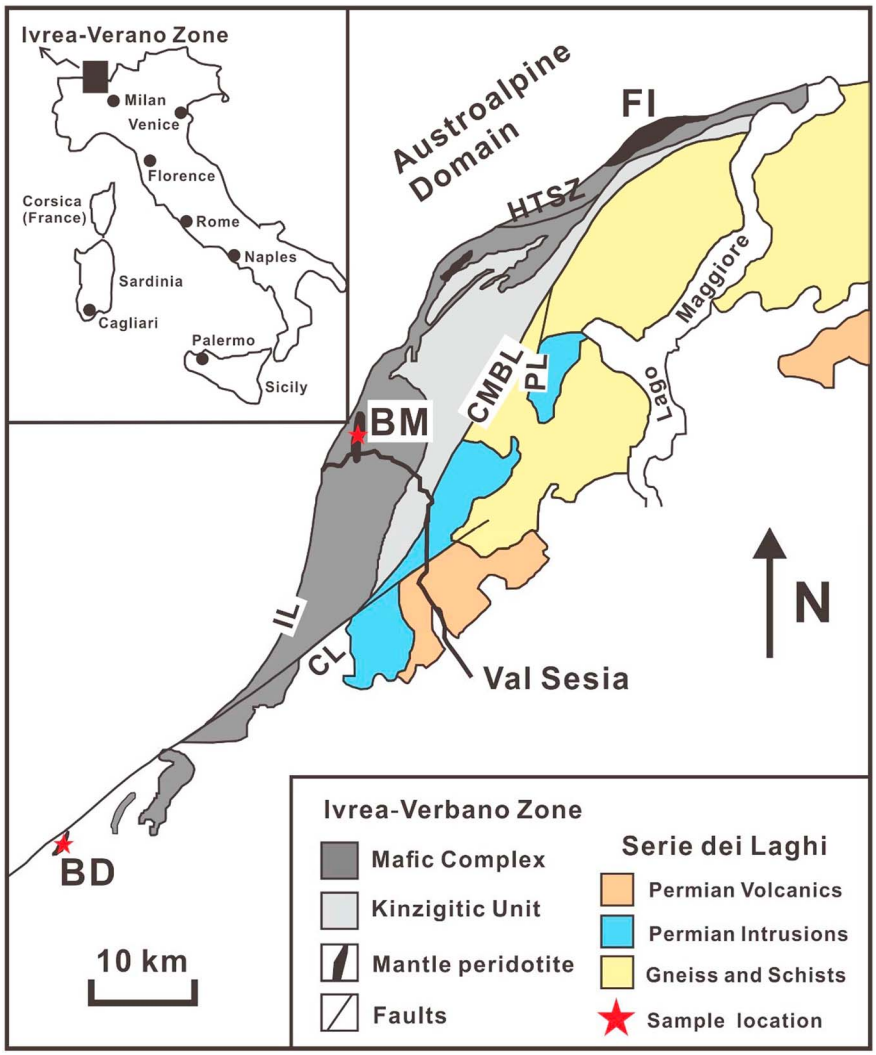

Figure 1. Geological map of the Ivrea-Verbano Zone with locations of the Baldissero (BD) and Balmuccia (BM) peridotite massifs marked with red stars (modified after Mazzucchelli et al., 2010). FI = Finero; CL = Cremoina line; IL = Insubric line; CMBL = Cossato-Mergozzo-Brissago line; PL = Pogallo line; HTSZ = high-temperature shear zone.

comparable to those of lherzolites, harzburgites, and dunites (Mazzucchelli et al., 2009; Mukasa & Shervais, 1999; Wang & Becker, 2015a). The MORB-like Sr-Nd-O isotopic compositions rule out any significant addition of crustal materials to the BD and BM peridotites (Hartmann & Hans Wedepohl, 1993; Obermiller, 1994; Mazzucchelli et al., 2009, 2010).

At BD and BM, harzburgites are rare and grade into lherzolites (Obermiller, 1994; Shervais & Mukasa, 1991) and dunites (Wang et al., 2013). In the BM massif, there are two main types of dunites, including thin dunite layers (<40 cm thick) and thick tabular dunites (150 × 50 m^2). The former commonly occur as "depletion zones" between pyroxenite dykes and lherzolites and are the results of melt extraction induced by intrusion of melts derived from a garnet-facies mantle (Rivalenti et al., 1995; Shervais & Mukasa, 1991). The latter are of replacive origin, represent the conduits for focused melt flow, and formed at the expense of their parental lherzolites as evidenced by the occurrence of lens of relict Cr-diopside websterites and Cr-spinel layers within them (Mazzucchelli et al., 2009; Shervais & Mukasa, 1991).

The BD and BM peridotite samples investigated here have been previously studied for the petrology, major elements, siderophile and chalcophile elements, and Sr-Nd-Os-Cu isotopic compositions (Huang et al., 2017; Obermiller, 1994; Rivalenti et al., 1995; Wang et al., 2013). They include 15 lherzolites, 3 harzburgites, and 3

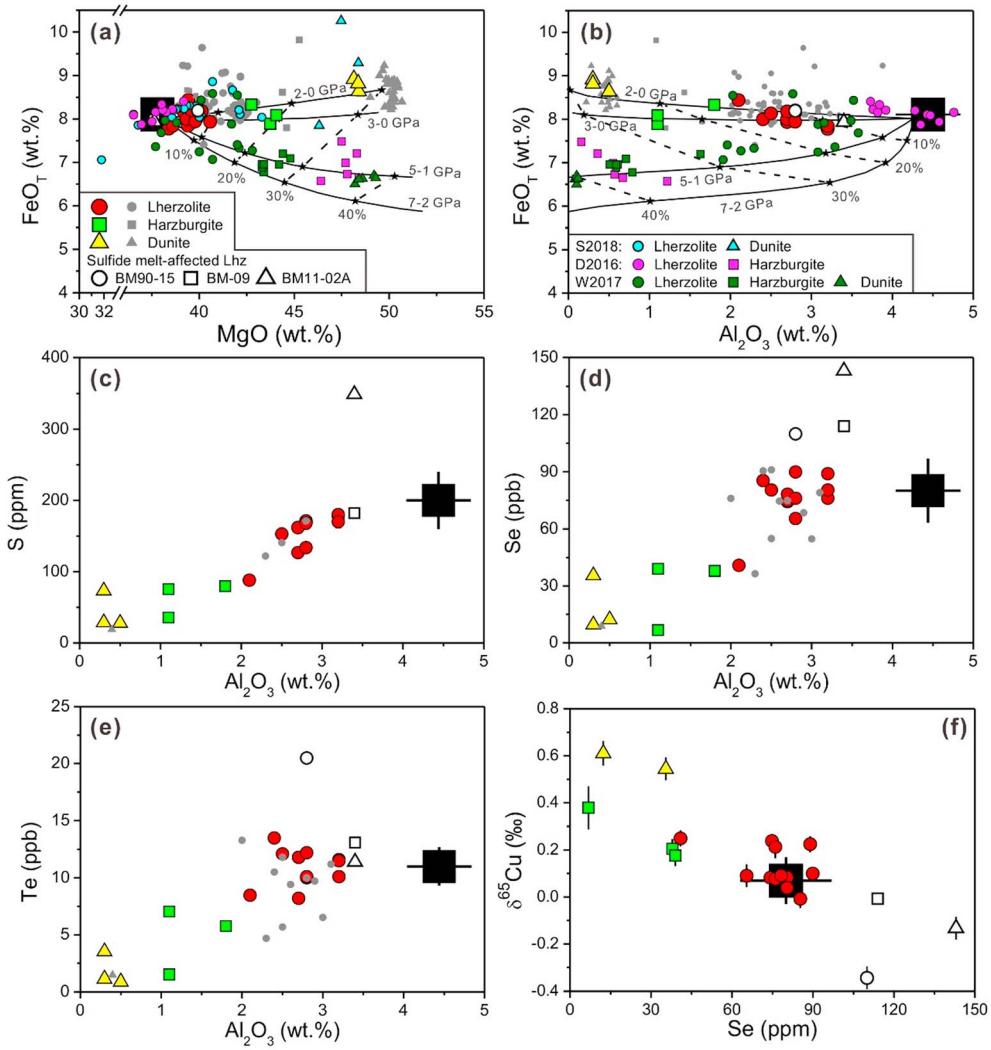

Figure 2. FeO$_T$ versus (a) MgO and (b) Al_2O_3; Al_2O_3 versus (c) S, (d) Se, (e) Te; and Se versus (f) δ^{65}Cu in the Baldissero and Balmuccia massif peridotites. Data for BD and BM samples are from previous studies (Hartmann & Hans Wedepohl, 1993; Huang et al., 2017; Mazzucchelli et al., 2009, 2010; Obermiller, 1994; Rivalenti et al., 1995; Wang et al., 2013). Large symbols in (a) denote the samples investigated in this study. For comparison, also plotted are data from Doucet et al. (2016, D2016), Wang et al. (2017, W2017), and Sossi et al. (2018, S2018). The black squares denote the primitive mantle values (Palme & O'Neill, 2014; Savage et al., 2015; Wang & Becker, 2013). In (a) and (b), the black lines denote experimentally determined compositions of residues formed during polybaric fractional melting of peridotite KR-4003 and the dashed lines show degrees of partial melting (Herzberg, 2004).

dunites, showing varying degrees of melt depletion and representing the entire range of variations of bulk compositions of peridotites reported in previous studies (Figures 2a and 2b). The dunites investigated here were collected from the tabular dunite bodies at BM, and their field occurrences were described in detail elsewhere (Wang et al., 2013). Dunite BM11-03A and harzburgite BM11-03B were collected ~20 cm distance from the gradational boundary of a local harzburgite-dunite transition zone. With decreasing orthopyroxene abundance, harzburgite grades into dunite. Dunite BM11-07A was sampled 40-cm distance from the contact to a pyroxenite dyke and dunite BM11-24A was collected 2-cm distance from a spinel-rich layer. All the studied samples are exceptionally fresh as indicated by the absence of secondary serpentine, no alteration of sulfide, low loss on ignition (typically <1 wt %), and the systematic variations of alteration-sensitive chalcophile elements (e.g., Cu, S, Se, and Te) with Al_2O_3 (Figures 2c–2e) (Huang et al., 2017; Obermiller, 1994; Wang et al., 2013).

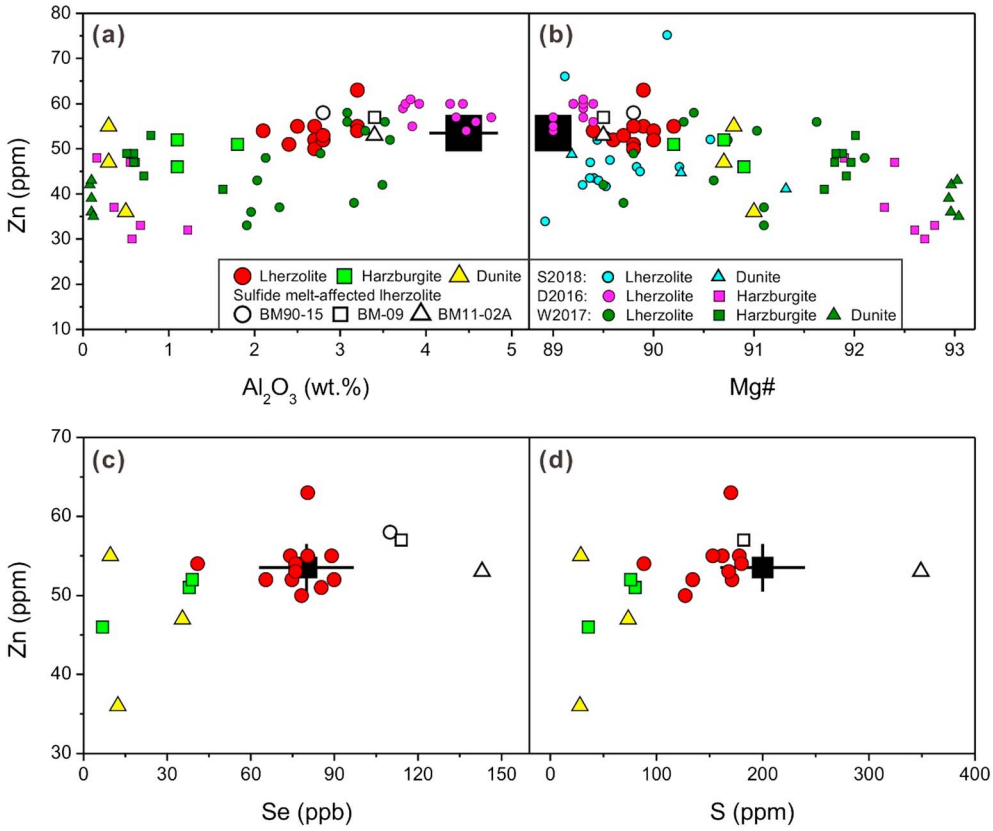

Figure 3. Zn versus (a) Al_2O_3, (b) Mg#, (c) Se, and (d) S in the Baldissero and Balmuccia massif peridotites. Data are from Wang et al. (2013). The black squares denote the primitive mantle values (Palme & O'Neill, 2014; Wang & Becker, 2013). D2016 = Doucet et al. (2016), W2017 = Wang et al. (2017), and S2018 = Sossi et al. (2018).

The lherzolites have Zn contents from 50 to 63 ppm, similar to or higher than those of harzburgites (46–52 ppm) and dunites (36–55 ppm; Figure 3). Three lherzolites (i.e., BM90-15, BM-09, and BM11-02A) with high S, Se, and Te contents but low δ^{65}Cu values (Figures 2c–2f) record a metasomatic event of sulfide melts (Huang et al., 2017; Wang et al., 2013). The BM tabular dunites have higher δ^{65}Cu, S/Se, and Se/Te ratios but lower S, Se, and Te contents (Figures 2c–2f) relative to their parental lherzolites, reflecting S-undersaturated silicate melt percolation (Huang et al., 2017; Wang et al., 2013). Thus, these samples allow us to assess the behavior of Zn isotopes during interactions of the mantle with different types of melts.

3. Analytical Methods

Bulk rock rare earth element (REE) contents were obtained by an ELAN DRCII inductively coupled plasma-mass spectrometry at the University of Science and Technology of China after double-distilled acid digestion (HNO_3 + HF + $HClO_4$) of ~50-mg sample powders in high-pressure Teflon bombs. Analytical procedures are adapted from Huang et al. (2012). The measured values of international U.S. Geological Survey standard BHVO-2 are well consistent with the recommended values within error (Table 1; Jochum & Nohl, 2008, and reference therein).

Zinc isotopic compositions were analyzed at the University of Science and Technology of China. Detailed procedures were described in Chen et al. (2016), and a brief description is given here. Sample powders were dissolved in a mixture of double-distilled concentrated HF + HNO_3 using high-pressure Teflon bombs in a furnace at 195 °C for ~96 hr for full digestion. Residues after dryness were then digested in a mixture of concentrated HCl + HNO_3 using PFA beakers (Savillex®) on a hotplate at 140 °C. This procedure has been proved to be efficient for completely dissolving spinel (Sossi et al., 2015; Wang et al., 2017). After complete dissolution and evaporation of the acid solution, the residues were refluxed with 1-mL 6 N HCl and then dried down to

Journal of Geophysical Research: Solid Earth

10.1002/2017JB015287

Table 1
Zinc Isotopic Compositions and REE Contents of the Baldissero and Balmuccia Peridotites

Sample	Rock[a] Type	δ^{66}Zn ‰	2SD[b]	δ^{68}Zn ‰	2SD	N[c]	Al_2O_3[d] wt %	Zn[d] ppm	La ppm	Ce ppm	Pr ppm	Nd ppm	Sm ppm	Eu ppm	Gd ppm	Tb ppm	Dy ppm	Ho ppm	Er ppm	Tm ppm	Yb ppm	Lu ppm
Baldissero																						
BD11-01	L	0.20	0.01	0.41	0.01	3	2.7	55	0.006	0.081	0.031	0.256	0.152	0.059	0.237	0.050	0.387	0.092	0.252	0.042	0.283	0.045
BD11-05	L	0.15	0.01	0.30	0.01	3	3.2	55	0.008	0.051	0.025	0.234	0.161	0.074	0.265	0.068	0.443	0.113	0.330	0.053	0.379	0.059
BD11-07	L	0.27	0.05	0.53	0.09	3	2.8	52	0.025	0.056	0.017	0.189	0.130	0.060	0.237	0.066	0.419	0.106	0.293	0.050	0.337	0.050
BD11-08	L	0.14	0.07	0.27	0.08	3	3.2	54	0.032	0.123	0.031	0.256	0.152	0.071	0.264	0.062	0.448	0.105	0.311	0.049	0.334	0.053
BD90-4	L	0.21	0.02	0.44	0.02	3	2.4	51	0.024	0.082	0.020	0.146	0.097	0.040	0.165	0.043	0.303	0.073	0.225	0.034	0.236	0.042
BD90-10	L	0.27	0.03	0.52	0.06	3	2.7	52	0.006	0.062	0.031	0.261	0.156	0.068	0.261	0.058	0.389	0.093	0.262	0.038	0.276	0.045
BD92-2	H	0.18	0.02	0.36	0.02	3	1.8	51	0.061	0.177	0.032	0.174	0.089	0.035	0.129	0.033	0.222	0.055	0.164	0.029	0.194	0.034
BD-17	H	0.43	0.04	0.89	0.04	3	1.1	46	0.031	0.077	0.014	0.059	0.020	0.012	0.035	0.007	0.036	0.011	0.026	0.007	0.055	0.010
Replicate[e]		0.42	0.02	0.83	0.04	3																
Balmuccia																						
BM90-15	L	0.18	0.02	0.36	0.03	3	2.8	58	0.010	0.034	0.011	0.115	0.090	0.045	0.180	0.047	0.341	0.082	0.254	0.039	0.257	0.041
BM-09	L	0.22	0.05	0.46	0.04	3	3.4	57	0.031	0.094	0.024	0.206	0.135	0.061	0.252	0.062	0.438	0.109	0.328	0.051	0.356	0.057
BM11-02A	L	0.13	0.02	0.28	0.03	3	3.4	53	0.022	0.070	0.016	0.137	0.099	0.049	0.227	0.055	0.377	0.100	0.282	0.046	0.337	0.054
BM11-04	L	0.19	0.04	0.40	0.07	3	2.5	55	0.018	0.042	0.013	0.111	0.098	0.048	0.174	0.041	0.296	0.078	0.215	0.034	0.214	0.038
BM11-08	L	0.21	0.04	0.44	0.06	3	3.2	63	0.011	0.054	0.019	0.186	0.132	0.059	0.220	0.056	0.391	0.097	0.292	0.044	0.301	0.053
BM11-09	L	0.23	0.06	0.50	0.09	3	2.7	50	0.002	0.022	0.013	0.144	0.121	0.054	0.208	0.054	0.356	0.087	0.268	0.042	0.299	0.047
BM11-10	L	0.21	0.02	0.41	0.05	3	2.8	52	0.002	0.023	0.013	0.152	0.108	0.061	0.230	0.060	0.384	0.102	0.298	0.048	0.314	0.050
BM11-11	L	0.18	0.01	0.37	0.01	3	2.1	54	0.033	0.131	0.027	0.180	0.081	0.039	0.131	0.033	0.222	0.055	0.173	0.030	0.190	0.036
Replicate[e]		0.17	0.03	0.36	0.03	3																
BM11-18	L	0.16	0.07	0.30	0.10	3	2.8	53	0.001	0.020	0.013	0.137	0.106	0.053	0.203	0.049	0.387	0.091	0.282	0.046	0.303	0.049
BM11-03B	H	0.28	0.02	0.55	0.06	3	1.1	52	0.041	0.122	0.023	0.113	0.046	0.013	0.055	0.012	0.087	0.020	0.059	0.011	0.079	0.014
BM11-07A	D	0.33	0.02	0.64	0.03	3	0.3	47	0.010	0.024	0.004	0.023	0.006	0.003	0.011	0.003	0.021	0.005	0.015	0.003	0.035	0.006
BM11-24A	D	0.46	0.02	0.94	0.04	3	0.5	36	0.004	0.014	0.002	0.017	0.006	0.001	0.008	0.001	0.014	0.004	0.012	0.002	0.014	0.005
Replicate		0.45	0.02	0.92	0.05	3																
BM11-03A	D	0.24	0.02	0.47	0.06	3	0.3	55	0.009	0.025	0.004	0.017	0.007	0.001	0.009	0.001	0.007	0.002	0.005	0.001	0.008	0.002
Replicate[e]		0.25	0.02	0.52	0.07	3																
BHVO-2	B	0.30	0.01	0.6	0.05	3			14.69	36.45	5.26	23.78	5.78	1.94	5.99	0.99	5.23	1.01	2.56	0.34	1.99	0.29
BCR-2	B	0.22	0.03	0.45	0.04	3																
BIR-1	B	0.22	0.02	0.45	0.06	3																
PCC-1	D	0.21	0.01	0.41	0.04	3																
RGM-1	R	0.30	0.02	0.60	0.03	3																

[a]L = Lherzolite, H = Harzburgite, D = Dunite, B = Basalt; R = Rhyolite. [b]2SD = two times the standard deviation of the population of n ($n \geq 3$) repeated measurements of the same solution. [c]N = numbers of repeated measurements of the same solution by MC-ICPMS. [d]Data are from Wang et al. (2013) with the exception of BM11-11 whose Zn content was determined by comparison of signal intensities with 200 ppb IRMM3702 Zn in this study. [e]Replicate = repeating sample digestion, column chemistry, and instrumental analysis.

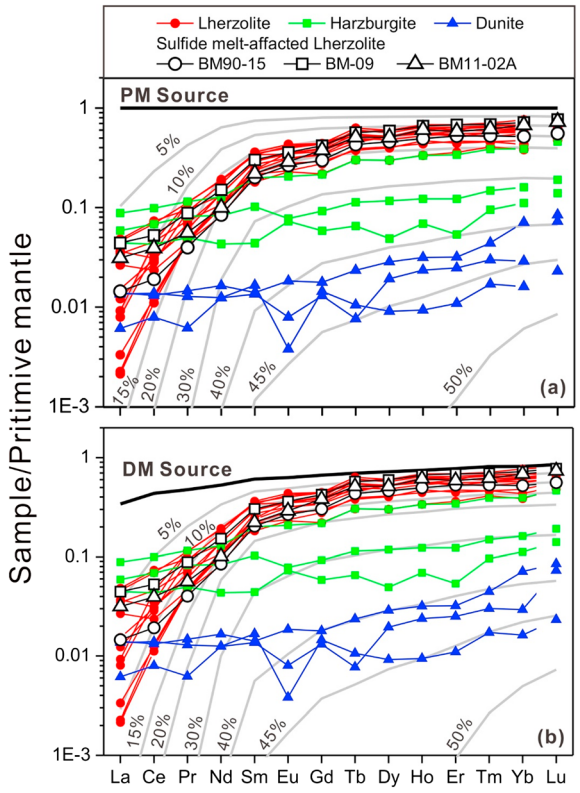

Figure 4. Primitive mantle-normalized rare earth element patterns of the Baldissero and Balmuccia massif peridotites. The light gray lines denote the modeled rare earth element (REE) patterns of residues generated by partial melting of the primitive (a, PM) and depleted mantle sources (b, DM). The numbers near the lines are degrees of partial melting. Fractional melting model was adapted from Johnson, Dick, and Shimizu (1990). The modal abundance of the source is 49% for olivine, 14% for orthopyroxene, 33% for clinopyroxene, and 4% for spinel, and the melting reaction is 0.28Opx + 0.67Cpx + 0.11Sp = 1Melt + 0.06Ol (Johnson et al., 1990). Partition coefficients are from the compilation of Niu and Hekinian (1997). Contents of REE for the PM (Palme & O'Neill, 2014) and DM (Salters & Stracke, 2004).

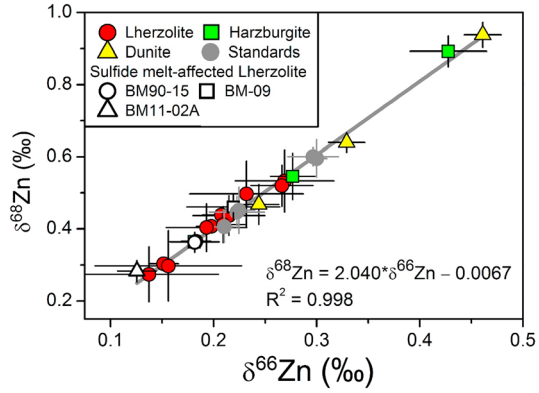

Figure 5. Three Zn isotope diagrams of standards and the Baldissero and Balmuccia massif peridotites. The slope of the gray regression line is 2.040, suggesting that Zn isotopes obey the mass-dependent fractionation law.

convert the residual solids into chloride. The final residues were taken up in 1-mL 6 N HCl prior to column chemistry. Zn was purified by anion exchange chromatography with Bio-Rad AG-MP-1 M strong anion resin in a 0.5 N HNO_3 media. The column chemistry was performed twice to efficiently purify Zn from interference cations. The Zn yields, based on analyses of Zn contents in the elution collected before and after the Zn cut, are >99%. The total procedural blanks range from 2.2 to 8.4 ng, negligible compared to ~2-μg Zn loaded onto the resin.

Zinc isotope ratios were determined using a Thermo-Fisher *Neptune Plus* multicollector inductively coupled mass spectrometry. A sample-standard bracketing method was applied to correct instrumental mass bias and time drifts (Chen et al., 2016; Maréchal et al., 1999). Five Zn isotopes (64, 66, 67, 68, and 70) were collected by L2, C, H1, H3, and H4 cups, respectively. A Ni(X) + Ni (Jet) cone assembly was used with the ^{64}Zn sensitivity of ~25 V/ppm. Zn isotope ratios are reported in standard δ-notation in per mil relative to JMC Lyon Zn standard 3-0749L: $\delta^{X}Zn = [(^{X}Zn/^{64}Zn)_{sample}/(^{X}Zn/^{64}Zn)_{JMC\ Lyon} - 1] \times 1{,}000‰$, where X = 66, 67, 68, or 70. During the course of this study, repeated analyses of IRMM3702 and JMC-Lyon 3-0749L yielded δ^{66}Zn of 0.27 ± 0.04‰ (2SD, *n* = 41) and 0.00 ± 0.05‰ (2SD, *n* = 70), respectively. Thus, the long-term external reproducibility for δ^{66}Zn is ±0.05‰ (2SD) for this study. The δ^{66}Zn of reference standards BHVO-2, BCR-2, BIR-1, and PCC-1 (Table 1) obtained in this study agree well within error with previously published values (Chen et al., 2013; Doucet et al., 2016; Moeller et al., 2012; Moynier et al., 2011, 2017; Petit et al., 2008; Sossi et al., 2015; Wang et al., 2017). This, combined with consistent results for repeated analyses (Table 1), assures the accuracy and precision of our data. In addition, we report for the first time the Zn isotopic composition of the reference material RGM-1 (δ^{66}Zn = 0.30 ± 0.02‰, 2SD) (Table 1).

4. Results

Zinc isotopic compositions and REE contents of the BD and BM peridotites are listed in Table 1. The harzburgites and dunites display middle to heavy REE (middle REE: Sm-Ho, HREE: Er-Lu) contents lower than but light REE (e.g., La and Ce) contents similar to or higher than those of the lherzolites (Figure 4). The lherzolites show a strong LREE depletion relative to HREE with $(La/Yb)_{PM}$ (subscript PM denotes Primitive-Mantle normalization) from 0.003 to 0.125, while the harzburgites and dunites have a relatively flat REE pattern with $(La/Yb)_{PM}$ from 0.197 to 0.842 (Figure 4). All types of peridotites have low REE contents with ΣREE from 0.10 to 2.93 ppm (Table 1).

In the plot of δ^{66}Zn versus δ^{68}Zn (Figure 5), the data define a linear line with a slope of 2.040, consistent with the value theoretically predicted based on mass differences of ^{66}Zn and ^{68}Zn (Schauble, 2004), suggesting that Zn isotopes obey the mass-dependent fractionation law. Hence, we only discuss the δ^{66}Zn in this study. Lherzolites have a narrow range of δ^{66}Zn from 0.13 to 0.27‰, while harzburgites and dunites display a larger range of δ^{66}Zn from 0.18 to 0.43‰ and from 0.24 to 0.46‰, respectively (Figure 6). Their δ^{66}Zn shows no correlations with indicators of melt extraction (e.g., Al_2O_3, Mg# = molar Mg/(Mg + Fe) × 100) (Figures 6a and 6b). For harzburgites and dunites, the δ^{66}Zn is

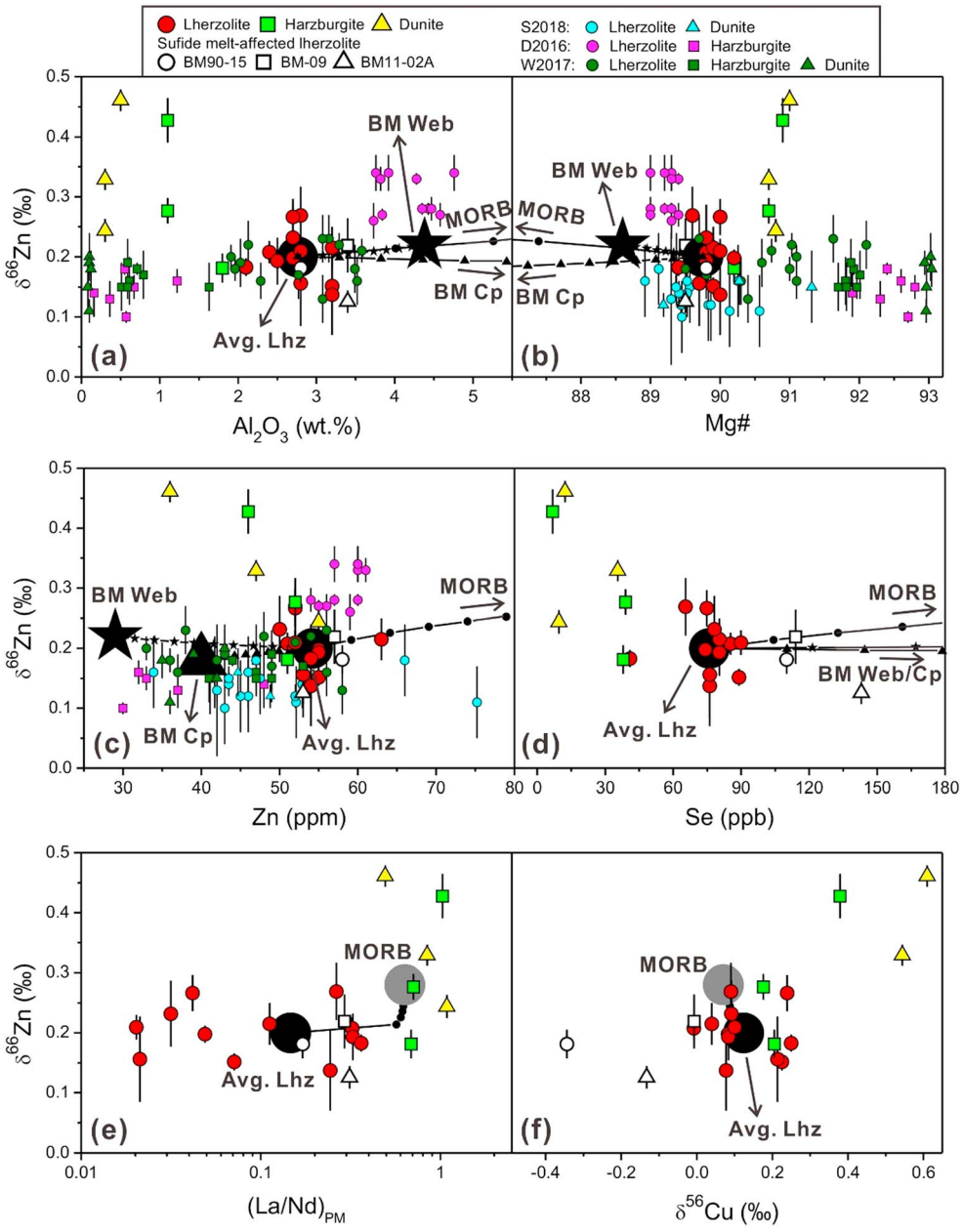

Figure 6. δ^{66}Zn versus (a) Al_2O_3, (b) Mg#, (c) Zn, (d) Se, (e) $(La/Nd)_{PM}$, and (f) δ^{65}Cu in the Baldissero and Balmuccia massif peridotites. Data from Al_2O_3, Mg#, Zn, Se, and δ^{65}Cu are from Wang et al. (2013) and Huang et al. (2017). The black lines/curves denote mixing (with 10% increment) between lherzolites (Avg. Lhz, black circles) with Cr-dioposide websterites (BM Web, black stars), Al-augite clinopyroxenites (BM Cp, black triangles), and MORB (gray solid circles). $(La/Nd)_{PM}$ denote PM-normalized ratios. D2016 = Doucet et al. (2016), W2017 = Wang et al. (2017), and S2018 = Sossi et al. (2018). See discussions in section 5.3.3 and input parameters in Table 2.

negatively correlated with Zn contents (Figure 6c). Harzburgites and dunites with high δ^{66}Zn show lower S, Se contents but higher δ^{65}Cu and $(La/Nd)_{PM}$ ratios relative to lherzolites (Figures 6d–6f).

5. Discussion

5.1. Effect of Partial Melting

Doucet et al. (2016) found that the δ^{66}Zn (~0.30‰) of fertile peridotites from Vitim and Tariat is higher than that (~0.14‰) of the refractory harzburgites from Udachnaya kimberlite. This finding led them to propose

that significant Zn isotope fractionation (up to 0.16‰ δ^{66}Zn) occurs during high degrees of melt extraction (>30%), which is controlled by the stability of clinopyroxene and garnet in the melting residues. It has been experimentally demonstrated that the modal abundances of clinopyroxene and garnet in the melting residues are determined by melting pressures (Herzberg, 2004; Walter, 1998). Thus, Doucet et al. (2016) suggested that Zn isotope fractionation during mantle melting is pressure-dependent. However, Wang et al. (2017) reported that peridotite residues, generated by 5–40% degrees of melting of a primitive mantle-like source with initial melting pressures of 1–5 GPa, have a homogeneous Zn isotopic composition (δ^{66}Zn = 0.18 ± 0.06‰, 2SD). This suggests that pressure does not influence Zn isotope fractionation during mantle melting.

Given that Zn substitutes for Fe and/or Mg in mantle minerals (Le Roux et al., 2010) due to the similar ionic radii of Zn^{2+} (0.74 Å), Mg^{2+} (0.72 Å), and Fe^{2+} (0.78 Å) (Shannon, 1976), Doucet et al. (2016) hypothetically proposed that intermineral Zn isotope fractionation follows the same order as Mg isotopes: $\delta^{66}Zn_{Spinel} \geq \delta^{66}Zn_{Clinopyroxene} > \delta^{66}Zn_{Orthopyroxene} > \delta^{66}Zn_{Olivine} > \delta^{66}Zn_{Garnet}$ (Huang et al., 2013). This led them to suggest that melting residues after preferential removal of clinopyroxene are enriched in ^{64}Zn relative to their source. However, Zn isotopic measurements for olivine, clinopyroxene, and orthopyroxene did not reveal the small isotope fractionation among these minerals (Wang et al., 2017), indicating that preferential removal of clinopyroxene is unlikely to cause significant Zn isotope fractionation during mantle melting. Wang et al. (2017) proposed that mantle melting could cause ~0.10‰ δ^{66}Zn fractionation based on higher δ^{66}Zn of MORBs (~0.28‰) than that of the unmetasomatic peridotites (~0.18‰), which was ascribed to preferential melting of isotopically heavy spinel from the peridotite residues ($\Delta^{66}Zn_{Spl\text{-}Ol} = \delta^{66}Zn_{Spl} - \delta^{66}Zn_{Ol}$ = 0.12 ± 0.07‰). However, Wang et al. (2017)'s model works only at high degrees (~20%) of mantle melting where spinel gets exhaustion. This is inconsistent with the widely accepted view that MORBs are formed by 5–20% melting of the upper mantle where spinel modal abundance barely changes (e.g., Hamlyn et al., 1985; Klein & Langmuir, 1987). Because Zn has a fourfold coordination (^{IV}Zn) in basaltic melts (Dumas & Petiau, 1986; Le Grand et al., 2000) and a sixfold coordination (^{VI}Zn) in olivine and pyroxene (Le Roux et al., 2010), Sossi et al. (2018) proposed that the difference in δ^{66}Zn between MORBs and peridotites may be ascribed to isotope fractionation between $^{IV}Zn^{2+}$and $^{VI}Zn^{2+}$, considering that the former has a shorter Zn–O bond and thus prefers heavier isotopes relative to the latter (Schauble, 2004).

Lherzolites at BD and BM have δ^{66}Zn ranging from 0.13 to 0.27‰, lighter than those of basalt-hosted off-craton lherzolite xenoliths (0.26 to 0.34‰, Doucet et al., 2016), but within errors overlapping with those of craton lherzolite xenoliths (0.13 to 0.23‰, Wang et al., 2017) and BM orogenic lherzolites measured by Sossi et al. (2018) (0.10 to 0.18‰) (Figures 6a–6c). The cause of Zn isotopic discrepancy between off-craton and craton/orogenic lherzolites is yet unknown (Sossi et al., 2018). Fractional melting model based on their PM-normalized REE patterns suggests that the BD and BM lherzolites are melting residues after ≤15% degrees of melting of a PM- or DM-like source (Figure 4), consistent with the previous results (Hartmann & Hans Wedepohl, 1993; Mazzucchelli et al., 2010; Mukasa & Shervais, 1999; Rivalenti et al., 1995). Our Zn isotope data show no systematic differences in δ^{66}Zn related to variable Al_2O_3 contents (Figure 6a), Mg# (Figure 6b), and $(La/Nd)_{PM}$ (Figure 6f) of the BD and BM lherzolites. This suggests that ≤15% degrees of melt extraction is unlikely to cause a detectable Zn isotope fractionation in the massif peridotites of the Ivrea-Verbano Zone (Italian Alps), consistent with the previous views that partial melting has a limited effect on the Zn isotopic compositions of the residual peridotites (Sossi et al., 2018; Wang et al., 2017) and that only high degrees of melt extraction (>30%) may significantly fractionate Zn isotopes (Doucet et al., 2016).

5.2. Effect of Sulfide Melt Addition

Lherzolites BM11-02A, BM90-15, and BM-09 have high S, Se, and Te contents and low δ^{65}Cu (Figures 2c and 2f and 3c and 3d), reflecting local addition of sulfide melts (Huang et al., 2017; Wang et al., 2013). They have similar Zn contents and δ^{66}Zn to the other lherzolites (Figures 3 and 6), suggesting that local addition of sulfide melts did not modify the Zn elemental and isotopic budget of peridotites at BM. This may be due to the very low Zn contents of sulfide melts. Sulfides in mantle peridotites mainly consist of Cu-Ni-Fe-S (≥99% by volume, Garuti et al., 1984; Lorand, 1989; Wang et al., 2013), which only contain a few Zn, usually below detection limits (Garuti et al., 1984).

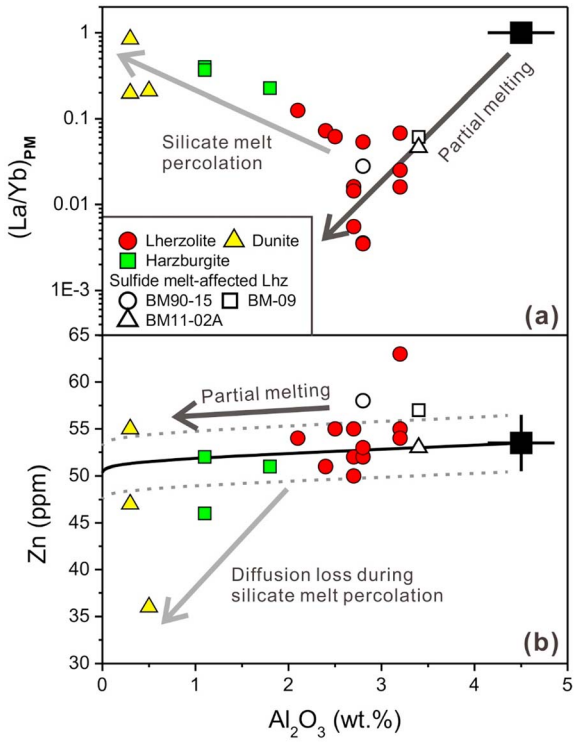

Figure 7. Al_2O_3 versus (a) $(La/Yb)_{PM}$ and (b) Zn in the Baldissero and Balmuccia massif peridotites, compared to the modeling results of mantle partial melting. Fractional melting model was used (Johnson et al., 1990). Procedures in detail are described in Figure 4. Partition coefficients of Zn are 0.96 for olivine, 0.45 for orthopyroxene, 0.33 for clinopyroxene, and 5.2 for spinel (Davis et al., 2013). Bulk partition coefficients of Al_2O_3 at various degrees of partial melting were calculated using the equation given by Niu (1997). The black line denotes the modeled results using the average values of primitive mantle, while the gray dashed lines are the upper and lower limits. The bold black and grey lines with arrows qualitatively illustrate the trends of partial melting and silicate melt percolation, respectively. Primitive mantle values (black squares) are taken from Palme and O'Neill (2014).

5.3. Origin of High δ^{66}Zn in Harzburgites and Dunites

5.3.1. Origin of Harzburgites and Dunites

Lherzolites studied here show a strong depletion of LREE relative to HREE with $(La/Yb)_{PM}$ of 0.003 to 0.125, consistent with 5–15% partial melting of a PM- or DM-like source in a fractional melting model (Figure 4). If lherzolites and harzburgites are the pure residuum of partial melting of the primitive mantle, harzburgites with lower Al_2O_3 and higher MgO contents generated by higher degrees of melt extraction should display lower LREE contents and $(La/Yb)_{PM}$ ratios relative to lherzolites because LREEs are more incompatible than HREE during mantle partial melting (Kelemen et al., 1992; Niu & Hekinian, 1997). Harzburgites at BD and BM display a relatively flat PM-Normalized REE patterns with higher La and Ce contents and $(La/Nd)_{PM}$ and $(La/Yb)_{PM}$ ratios (0.226–0.399) relative to the parental lherzolites and melts generated by partial melting of a PM-like source (Figures 4, 6f, and 7a). Such features were also observed in most ophiolitic and abyssal harzburgites (Kelemen et al., 1992; Niu & Hekinian, 1997). In addition, Rivalenti et al. (1995) found that at BM, peridotites and clinopyroxenes in contact with Cr-diopside websterite dykes have higher LREE contents and $(La/Yb)_{PM}$ ratios compared to peridotites and clinopyroxenes away from dykes. These authors attributed such features to melt extraction induced by percolation of melts derived from the deep mantle with diffusive redistribution of LREE between melts and peridotites. Thus, the studied harzburgites likely originated from melt percolation-induced partial melting of the parental lherzolites.

Field, petrological, and geochemical evidence indicate that tabular dunites at BM are of replacive origin and formed by S-undersaturated silicate melt percolation of the parental lherzolites at high melt/rock ratios (Huang et al., 2017; Mazzucchelli et al., 2009; Wang et al., 2013). Silicate melt percolation at high melt/rock ratios results in dissolution of pyroxene + sulfide ± spinel and precipitation of olivine, leading to the formation of replacive dunites (Kelemen, Shimizu, & Salters, 1995). These mineral dissolution and precipitation processes (pyroxene + sulfide ± spinel + melt1 → olivine + melt2) are inferred to explain the lower incompatible element (e.g., Al, Cu, S, Se, Te, M-HREE, Re, Pt, and Pd) contents, but variably higher compatible PGE (e.g., Ir, Ru, and Rh) contents, δ^{65}Cu, S/Se, and Se/Te of the dunites relative to the parental lherzolites as well as the similarity of Mg# between harzburgites and dunites (Figures 2 and 3b; Huang et al., 2017; Wang et al., 2013; this study).

5.3.2. Comparison With Previous Studies

Except for harzburgite BD92-2, the δ^{66}Zn of harzburgites and dunites studied here (0.24 to 0.46‰) are higher than those of harzburgites and dunites measured by previous studies (0.10 to 0.20‰; Figures 6a–6c; Doucet et al., 2016; Sossi et al., 2018; Wang et al., 2017). In the study of Doucet et al. (2016), harzburgites were collected from the Udachnaya kimberlite (Siberian craton) and represent pristine residues of high-degree (30–40%) polybaric melting of a PM-like source at high pressures (7–4 GPa; (Figures 2a and 2b; Doucet et al., 2012). Harzburgites and dunites in Wang et al. (2017) were collected from the Raobazhai peridotite complex in the Dabie-Sulu orogenic belt that was formed by Triassic continental collision between the Yangtze and North China Cratons (Li et al., 1993). The Raobazhai peridotites form part of the mantle wedge above the subducting Yangtze Craton during Triassic collision and are now tectonically exposed within Neoproterozoic orthogneisses (Zheng et al., 2008). They represent refractory residues after high-degree (25–40%) melt extraction from a PM-like source (Figures 2a and 2b) and then were metasomatized by fluids/melts released from the subducting Yangtze Craton (Zheng et al., 2008). Such metasomatism caused an enrichment of large ion lithophile elements (such as K, Rb, Ba, and Sr) but a limited effect on major elements and Zn isotopes of the Raobazhai peridotites (Wang et al., 2017; Zheng et al., 2008). Higher Mg# in dunites than in harzburgites

at Raobazhai (Figure 6b; Wang et al., 2017) are consistent with the view that they are partial melting residues (Zheng et al., 2008). Accordingly, Wang's harzburgites and dunites have similar δ^{66}Zn to their lherzolites (Figures 6a–6c) because partial melting results in insignificant Zn isotope fractionation in residual peridotites (Sossi et al., 2018; Wang et al., 2017; this study). Our harzburgites and dunites had experienced silicate melting percolation that elevated their δ^{66}Zn values (see section 5.3.5).

Sossi's and our dunites were collected from different parts of the BM peridotite massif and have different chemical compositions (Figure 2a). Our dunites were sampled from the tabular dunite bodies at BM, and the sampling coordinates can be found in Wang et al. (2013). They were classified by Wang et al. (2013) based on petrology and whole rock chemistry (including all major elements). They have compositions similar to those of the BM dunites measured by previous studies (Mazzucchelli et al., 2009; Rivalenti et al., 1995; Figures 2a and 2b), and their Mg# are higher than those of lherzolites from the same massif (Figures 3b and 6b). They originated from percolation of the parental lherzolites by S-undersaturated silicate melts at high melt/rock ratios (Huang et al., 2017; Mazzucchelli et al., 2009; Wang et al., 2013). Sossi et al. (2018) did not provide the coordinates of samples and reported that their peridotites were collected along the Sesia River intersecting the BM massif. Apart from Zn isotopic data, Sossi et al. (2018) only presented MgO, FeO_T, and Zn contents of peridotites and subdivided samples with $>$46 wt % MgO to dunites. However, in the plot of MgO versus FeO (Figure 2a), Sossi's dunites deviate significantly from the field defined by the BM dunites in previous studies (Mazzucchelli et al., 2009; Rivalenti et al., 1995; Wang et al., 2013). In addition, except for dunite BD31, Sossi's dunites have Mg# similar to those of the BD and BM lherzolites (Figures 3b and 6b). All these evidence suggest that Sossi's and our dunites experienced different geological processes and thus have different origins. This may explain why Sossi's and our dunites do not have similar Zn isotopic compositions (Figures 6a–6c).

5.3.3. Mixing With Deep-Seated Melts

Recycling of isotopically heavy sedimentary carbonates (up to 1.34‰; Pichat et al., 2003) and pegmatites (up to 0.88‰; Telus et al., 2012) into the mantle has been proposed to explain the high δ^{66}Zn of continental basalts (up to 0.60‰) and wehrlites (up to 0.42‰) from eastern China (Liu et al., 2016; Wang et al., 2017). However, such interpretation is inconsistent with the MORB-like Sr-Nd-O isotopic compositions and strongly depleted PM-normalized REE patterns of the BD and BM peridotites, which reflect no or limited (if any) modification by crustal materials (e.g., Hartmann & Hans Wedepohl, 1993; Obermiller, 1994; Mazzucchelli et al., 2009, 2010; this study).

Harzburgites and dunites investigated here formed via percolation of lherzolites by melts derived from the deep mantle in the garnet stability (see section 5.3.1). It is thus necessary to assess whether mixing of such deep-seated melts with lherzolites can explain the high δ^{66}Zn of harzburgites and dunites (Figure 6). Mazzucchelli et al. (2009) proposed that the deep-seated melts involved in the BM dunite genesis were related to Cr-diopside websterites based on the similarity of Sr-Nd isotope ratios of clinopyroxene separates. The Cr-diopside websterites and younger Al-augite clinopyroxenites cumulated from primitive melts (i.e., deep-seated melts) of similar compositions, while the Al-augite clinopyroxenites represent more evolved differentiation stages, as revealed by crosscutting relationships, clinopyroxene trace element patterns, and whole-rock highly siderophile and chalcogen element contents (Rivalenti et al., 1995; Sinigoi et al., 1983; Wang & Becker, 2015a). The primitive melts should have chemical compositions between those of Cr-diopside websterites and Al-augite clinopyroxenites (Wang & Becker, 2015a). Considering that pyroxenites at BM have large compositional variations but similar element distribution patterns within individual Cr-diopside and Al-augite suites (Mazzucchelli et al., 2009; Mukasa & Shervais, 1999; Rivalenti et al., 1995; Wang & Becker, 2015a), we here assumed that the primitive melts have three different compositions for mixing calculations, including the Cr-diopside websterite average, the Al-augite clinopyroxenite average, and a MORB-like value. The modeled parameters for mixing are listed in Table 2.

Compared to lherzolites studied here Cr-diopside websterites and Al-augite clinopyroxenites have similar δ^{66}Zn, higher Al_2O_3 and Se contents, but lower Mg# and Zn contents, while MORBs have similar δ^{65}Cu; higher δ^{66}Zn, Al_2O_3, Zn, Se, and ΣREE (56.8 ppm, Hofmann, 1988) contents; and higher $(La/Nd)_{PM}$ but lower Mg# (Table 2). Mixing of melts with either a BM pyroxenite-like composition or a MORB-like composition into lherzolites are unlikely to produce the elemental and isotopic compositions of the BM and BD harzburgites and dunites (Figure 6).

Table 2
Input Parameters for Mixing Calculations

	Al_2O_3 wt %	MgO wt %	FeO_T wt %	Mg#	La ppm	Nd ppm	Se ppb	Cu ppm	Zn ppm	$\delta^{65}Cu$ ‰	$\delta^{66}Zn$ ‰
Lherzolite[a]	2.76	39.51	8.04	0.898	0.01	0.188	75.9	27.9	54.2	0.12	0.20
Websterite[b]	4.38	22.32	5.12	0.886			532		29		0.22
Clinopyroxenite[c]	8.10	19.54	5.66	0.860			419		40		0.18
N-MORB[d]	15.26	7.58	10.43	0.564	3.60	11.20	360	85.67	103.7	0.07	0.28

[a]Averages of lherzolites that were not affected by sulfide melt addition (Huang et al., 2017; Wang et al., 2013; this study). [b]Averages of Cr-diopside websterites (Wang & Becker, 2015a; Sossi et al., 2018). [c]Averages of Al-augite clinopyroxenites (Sossi et al., 2018; Wang & Becker, 2015a). [d]Major elements and REE (Hofmann, 1988); average Se, Cu, and Zn contents of 616 MORB samples (Jenner & O'Neill, 2012); $\delta^{66}Cu$ (Liu et al., 2015; Savage et al., 2015); and $\delta^{66}Zn$ (Wang et al., 2017).

5.3.4. Differential Dissolution of Minerals

Mineral dissolution reactions occurred during the formation of the harzburgites and dunites investigated in this study (see section 5.3.1). Their high $\delta^{65}Cu$ values were attributed by Huang et al. (2017) to preferential dissolution of sulfides that predominate the Cu budget of peridotites (Wang & Becker, 2015b) and have lighter Cu isotopic compositions relative to coexisting silicate minerals and oxides (Huang et al., 2016; Savage et al., 2015). However, two lines of evidence suggest that the high $\delta^{66}Zn$ of harzburgites and dunites cannot be explained by differential dissolution of pyroxene, spinel, and sulfide and precipitation of olivine during S-undersaturated silicate melt percolation. First, sulfides have a negligible influence on the Zn isotopic budget of peridotites as discussed in section 5.2. Second, mass balance showed that spinel only accounts for $<5\%$ (Le Roux et al., 2010) to $<20\%$ (O'Reilly et al., 1991) the total Zn budget of a peridotite. Zn isotopic measurements revealed that pyroxene, olivine, and whole-rock peridotite have similar $\delta^{66}Zn$, although spinel has slightly higher $\delta^{66}Zn$ compared to coexisting Fe-Mg silicates with $\Delta^{66}Zn_{Spl\text{-}Ol} = 0.12 \pm 0.07‰$ (Wang et al., 2017). All these evidence suggest that Fe-Mg silicates predominantly control the Zn isotopic budget of a peridotite. Thus, preferential dissolution of pyroxene and spinel and precipitation of olivine should not significantly modify the whole rock Zn isotopic compositions.

5.3.5. Diffusion-Driven Zn Isotope Fractionation During Silicate Melt Percolation

Melt percolation can result in significant isotopic variations of Li, Mg, Fe, Ca, and Cu in mantle peridotites (e.g., Huang et al., 2017; Kang et al., 2017; Rudnick & Ionov, 2007; Weyer & Ionov, 2007; Zhao et al., 2017). Both equilibrium and kinetic isotope fractionation could occur during melt percolation, and the magnitude of kinetic isotope fractionation depends on different diffusivities of isotopes and is usually much larger than that observed in equilibrium processes at high temperatures (Sossi, Nebel, & Foden, 2016, and references therein). As partial melting and differential dissolution of minerals cannot cause significant $\delta^{66}Zn$ fractionation in residual peridotites (Sossi et al., 2018; this study), the high $\delta^{66}Zn$ of harzburgites and dunites (Figure 6) most likely result from diffusion-driven kinetic isotope fractionation during melt percolation in the mantle. A fractional melting model (Figure 7b) indicates that the low Zn contents of some harzburgites and dunites cannot be explained by high degrees of partial melting of the PM and that diffusion loss of Zn occurred during S-undersaturated silicate melt percolation. Thus, the negative correlation between $\delta^{66}Zn$ and Zn contents of harzburgites and dunites (Figure 6b) can be attributed to isotope fractionation caused by diffusion loss of Zn from the peridotites to the percolating silicate melts. As lighter isotopes diffuse faster than heavier ones (Richter et al., 2003), preferential diffusion of ^{64}Zn to the percolating silicate melts results in coupled depletion of Zn and elevation of $\delta^{66}Zn$ observed in the BD and BM harzburgites and dunites (Figure 6b).

Diffusion experiments by equilibrating a San Carlos olivine with a synthetic silicate melt showed that Zn could diffuse out of olivine to the silicate melt (Spandler & O'Neil, 2010). The BM dunites are predominantly composed of olivine (modal abundance of $\geq 95\%$) with minor pyroxene, spinel, and sulfide (Mazzucchelli et al., 2009; Wang et al., 2013), and thus, their Zn elemental and isotopic compositions are dominantly controlled by olivine. Diffusion of Zn out of olivine determined the $\delta^{66}Zn$ of the BM dunites. To quantify how Zn isotope ratios were changed in dunites by diffusion of Zn out of olivine, we applied a model similar to that used by Lai et al. (2015). In this model, olivine is assumed to be a sphere in geometry with isotopic diffusion, and the melts act as an infinite reservoir that defines a fixed Zn content at the surface (or rim) of the olivine grain. The latter assumption may be reasonable because dunite channels are efficient conduits for focused flow

Table 3
Input Parameters for Zn Isotopic Diffusion in a Spherical Olivine

	C_i (ppm)[a]	C_r (ppm)[b]	D (m^2/s)[c]	a (mm)[d]	β_{Zn}[e]	δ^{66}Zn (‰)[f]
Melts	10, 20, 30					
Olivine	54.2 ± 6.5	9.6	1.78×10^{-15}	1.5	0.015, 0.03	0.20 ± 0.08
		19.2			0.04, 0.05	
		28.2			0.06, 0.07	

[a]As the Zn content of the percolating melts is lower than that of the dunite BM11-24A, its Zn content is set as 10, 20, and 30 ppm. The average Zn content of the parental lherzolites of dunites investigated here is taken as the initial olivine Zn content because it dominates the Zn budget of peridotites. [b]The Zn content at surface of olivine is calculated using the Zn content of the percolating melts and olivine-melt partition coefficients (K_D = 0.96; Davis et al., 2013). [c]The Zn diffusion coefficients in olivine is taken from Spandler and O'Neil (2010). [d]The radius of olivine is assumed to 1.5 mm, the midvalue of olivine in an equigranular-foliate matrix in the lherzolite (Shervais & Mukasa, 1991). [e]The assumed kinetic Zn isotope fractionation factors in olivine. [f]The initial olivine Zn isotopic composition is represented by the average of the BD and BM lherzolites (0.20 ± 0.08‰, 2SD), similar to that of olivine from the unmetasomatic peridotites (0.15 ± 0.06‰, 2SD, Wang et al., 2017).

of large volumes of melts (Kelemen, Shimizu, & Salters, 1995). The flow structures in the Cr-spinel layers suggest that the percolating melt flow rate and melt/rock ratios are sufficiently high during the formation of the BM dunite channels (Mazzucchelli et al., 2009). Specifically, the average element content of a spherical olivine grain after time t (C_t) can be calculated from the following equation defined by Crank (1975):

$$C_t = C_i + \frac{6(C_i - C_r)}{\pi^2} \sum_{n=1}^{\infty} \frac{1}{n^2} \exp\left(\frac{-Dtn^2\pi^2}{a^2}\right) \quad (1)$$

where C_i is the initial Zn content of olivine, C_r is the constant Zn content at the surface of olivine that is in equilibrium with the percolating melts, a is the radius of the olivine, and D is the diffusion coefficient of Zn in olivine.

Kinetic isotope fractionation induced by diffusion is related to the slightly different diffusion coefficients of different isotopes (Huang et al., 2010; Richter et al., 2003). For two isotopes (1 and 2) of one element, the ratio of their diffusion coefficients is

$$\frac{D_2}{D_1} = \left(\frac{m_1}{m_2}\right)^{\beta} \quad (2)$$

where m_1 and m_2 are their atomic masses, D_1 and D_2 are their diffusion coefficients, and β is the kinetic isotope fractionation factor. For Zn isotopes in this study, equation (2) can be specifically expressed as

$$\frac{D_{66Zn}}{D_{64Zn}} = \left(\frac{m_{64Zn}}{m_{66Zn}}\right)^{\beta_{Zn}} \quad (3)$$

According to the equations described above, the Zn isotopic composition of melt-affected olivine depends dominantly on four variables, including C_i, C_r, D, and β_{Zn}. In our approach, the average Zn content of the lherzolites investigated here (54.2 ± 6.5 ppm, 2SD, N = 15) is set as C_i, because they are the protoliths of the BM dunites and their bulk-rock Zn contents are largely controlled by olivine (Le Roux et al., 2010). The experimentally determined diffusion coefficient D is 1.78×10^{-15} m^2/s (Spandler & O'Neil, 2010). The C_r can be calculated by dividing the Zn content of the percolating melts (expressed as $[Zn]_{melt}$) with olivine-melt Zn partition coefficients (K_P = 0.96; Davis et al., 2013). The percolating melts should have Zn content lower than that of dunite BM11-24A (36 ppm, Table 1), because elements diffuse usually following chemical activity gradients (Richter et al., 2003). Because the chemical compositions of the percolating melts are between those of Cr-diopside websterites and younger Al-augite clinopyroxenites (see section 5.3.3; Wang & Becker, 2015a), the low $[Zn]_{melt}$ is also supported by the low Zn contents of two types of pyroxenites (12 out of 17 pyroxenite samples have Zn contents from 22 to 35 ppm; Wang & Becker, 2015a). To explore the effect of the $[Zn]_{melt}$ on the Zn isotopic composition of olivine, we assume a variable $[Zn]_{melt}$ from 10 to 30 ppm. To the best of our knowledge, no β_{Zn} in olivine has been reported in literature. Thus, the β_{Zn} was set as 0.015, 0.03, 0.04, 0.05,

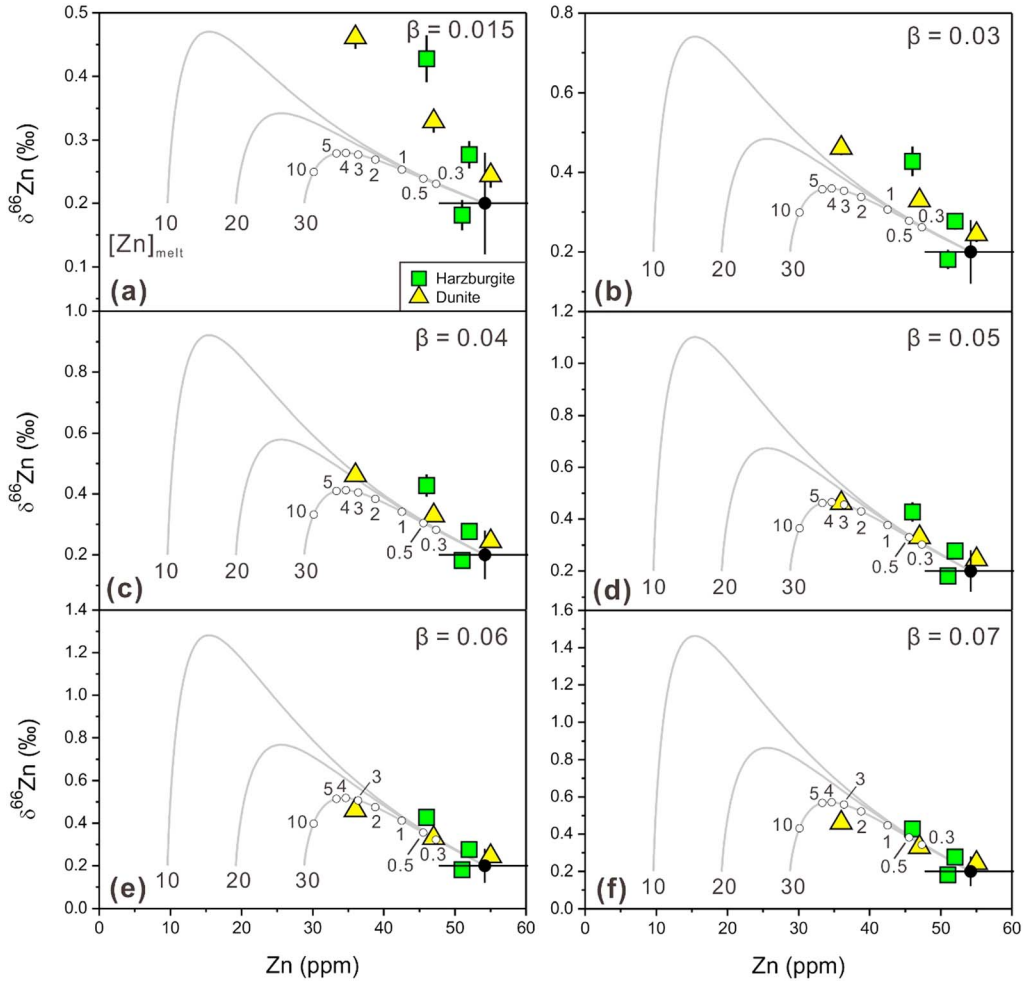

Figure 8. Diffusion-driven variations of olivine Zn contents and δ^{66}Zn (curves) during melt percolation with different Zn contents, compared to those of the dunites and harzburgites from the Balmuccia peridotite massif. The black solid circles denote the initial olivine Zn content and δ^{66}Zn (54.2 ± 6.5 ppm versus 0.20 ± 0.08‰, 2SD). The numbers at the end of the curves denote the assumed Zn contents of the percolating melts ($[Zn]_{melt}$), and near the curve for $[Zn]_{melt}$ = 30 ppm are the diffusion time (year). The β_{Zn} in olivine was arbitrarily set as 0.015, 0.03, 0.04, 0.05, 0.06, and 0.07. The modeling procedures are described in section 5.3.5, and input parameters are listed in Table 3.

0.06, and 0.07. In addition, the initial δ^{66}Zn of olivine is set to be 0.20‰ (the average of the BD and BM lherzolites), similar to that of olivine from the unmetasomatic peridotites (0.15 ± 0.06‰, 2SD; Wang et al., 2017). All input parameters for diffusion modeling can be found in Table 3, and the Matlab script is given in the supporting information.

The simulation results in Figure 8 show the modeling Zn elemental and isotopic compositions of olivine as a function of diffusion time with variable $[Zn]_{melt}$ and β_{Zn} in olivine. The results are compared to those of the harzburgites and dunites. The Zn isotopic data of the dunites and harzburgites can be explained by diffusion-driven isotope fractionation at β_{Zn} = 0.05–0.06 and 0.06–0.07, respectively, with 0.3 to 4-year durations of melt percolation when a = 1.5 mm and $[Zn]_{melt}$ = 30 ppm. The modeling results show that the duration of melt percolation largely depends on the radius of olivine assumed, but the inferred β_{Zn} in olivine is almost unaffected by the input parameters, such as $[Zn]_{melt}$ and a. The empirical β_{Zn} (0.05–0.06) obtained here is in the range of β_{Fe} (0.05–0.30) inferred from Fe isotopic zoning in natural olivines (Oeser et al., 2015; Sio et al., 2013; Teng et al., 2011). Such coincidence may be due to the similar ionic radius of divalent Zn (Zn^{2+}, 0.74 Å) and ferrous Fe (Fe^{2+}, 0.78 Å) in a sixfold coordination cation site, which enhances substituting Fe^{2+} by Zn^{2+} in olivine (Le Roux et al., 2010).

6. Conclusions

High-precision Zn isotopic compositions were determined for a suit of well-characterized orogenic peridotites from the BD and BM peridotite massifs in the Italian Southern Alps. The following conclusions can be drawn:

1. The lack of correlations between δ^{66}Zn and indicators of melt extraction (e.g., Al_2O_3 and Mg#) indicates limited Zn isotope fractionation during 5–15% partial melting of the mantle, consistent with the results of Doucet et al. (2016), Wang et al. (2017), and Sossi et al. (2018).
2. Lherzolites affected by sulfide melt percolation show similar Zn isotopic compositions to the other normal ones, suggesting that sulfide melt percolation is unlikely to cause significant Zn isotopic variations in the mantle.
3. The high δ^{66}Zn values (up to 0.46‰) of harzburgites and dunites are attributed to diffusion-driven kinetic isotope fractionation during S-undersaturated, Zn-depleted silicate melt percolation in the mantle. An empirical β_{Zn} (0.05–0.06) in olivine is obtained using a diffusion model based on the negative correlation of δ^{66}Zn and Zn contents in the replacive dunites at BM.

Acknowledgments
This study is financially supported by grants from the National Key K & D Program of the MOST (2016YFC0600404) and the National Natural Science Foundation of China (41773002, 41573018, and 41325011). We thank Z.-C Wang and H. Becker for providing samples, C. Zhou for help with the Matlab program, and H.-M. Yu for help with Zn isotope analyses. The data for this paper are listed in Tables 1–3 and related references and available for contacting the corresponding author at jianhuang@ustc.edu.cn.

References

Albarède, F. (2004). The stable isotope geochemistry of copper and zinc. *Reviews in Mineralogy and Geochemistry*, *55*(1), 409–427. https://doi.org/10.2138/gsrmg.55.1.409

Bodinier, J. L., & Godard, M. (2014). 3.4—Orogenic, ophiolitic, and abyssal peridotites A2—Holland, Heinrich D. In K. K. Turekian (Ed.), *Treatise on geochemistry* (2nd ed., pp. 103–167). Oxford: Elsevier. https://doi.org/10.1016/B978-0-08-095975-7.00204-7

Chen, H., Savage, P. S., Teng, F.-Z., Helz, R. T., & Moynier, F. (2013). Zinc isotope fractionation during magmatic differentiation and the isotopic composition of the bulk earth. *Earth and Planetary Science Letters*, *369–370*, 34–42.

Chen, S., Liu, Y., Hu, J., Zhang, Z., Hou, Z., Huang, F., & Yu, H. (2016). Zinc isotopic compositions of NIST SRM 683 and whole-rock reference materials. *Geostandards and Geoanalytical Research*, *40*(3), 417–432. https://doi.org/10.1111/j.1751-908X.2015.00377.x

Crank, J. (1975). *The mathematics of diffusion* (2nd ed.). Oxford: Clarendon Press.

Davis, F. A., Humayun, M., Hirschmann, M. M., & Cooper, R. S. (2013). Experimentally determined mineral/melt partitioning of first-row transition elements (FRTE) during partial melting of peridotite at 3.0 GPa. *Geochimica et Cosmochimica Acta*, *104*, 232–260. https://doi.org/10.1016/j.gca.2012.11.009

Doucet, L. S., Ionov, D. A., Golovin, A. V., & Pokhilenko, N. P. (2012). Depth, degrees and tectonic settings of mantle melting during craton formation: Inferences from major and trace element compositions of spinel harzburgite xenoliths from the Udachnaya kimberlite, central Siberia. *Earth and Planetary Science Letters*, *359–360*, 206–218.

Doucet, L. S., Mattielli, N., Ionov, D. A., Debouge, W., & Golovin, A. V. (2016). Zn isotopic heterogeneity in the mantle: A melting control? *Earth and Planetary Science Letters*, *451*, 232–240. https://doi.org/10.1016/j.epsl.2016.06.040

Dumas, T., & Petiau, J. (1986). EXAFS study of titanium and zinc environments during nucleation in a cordierite glass. *Journal of Non-Crystalline Solids*, *81*(1-2), 201–220. https://doi.org/10.1016/0022-3093(86)90270-X

Garuti, G., Gorgoni, C., & Sighinolfi, G. P. (1984). Sulfide mineralogy and chalcophile and siderophile element abundances in the Ivrea-Verbano mantle peridotites (western Italian Alps). *Earth and Planetary Science Letters*, *70*(1), 69–87. https://doi.org/10.1016/0012-821X(84)90210-3

Hamlyn, P. R., Keays, R. R., Cameron, W. E., Crawford, A. J., & Waldron, H. M. (1985). Precious metals in magnesian low-Ti lavas: Implications for metallogenesis and sulfur saturation in primary magmas. *Geochimica et Cosmochimica Acta*, *49*(8), 1797–1811. https://doi.org/10.1016/0016-7037(85)90150-4

Hartmann, G., & Hans Wedepohl, K. (1993). The composition of peridotite tectonites from the Ivrea Complex, northern Italy: Residues from melt extraction. *Geochimica et Cosmochimica Acta*, *57*(8), 1761–1782. https://doi.org/10.1016/0016-7037(93)90112-A

Herzberg, C. (2004). Geodynamic information in peridotite petrology. *Journal of Petrology*, *45*(12), 2507–2530. https://doi.org/10.1093/petrology/egh039

Hofmann, A. W. (1988). Chemical differentiation of the Earth: The relationship between mantle, continental crust, and oceanic crust. *Earth and Planetary Science Letters*, *90*(3), 297–314. https://doi.org/10.1016/0012-821X(88)90132-X

Huang, F., Chakraborty, P., Lundstrom, C. C., Holmden, C., Glessner, J. J. G., Kieffer, S. W., & Lesher, C. E. (2010). Isotope fractionation in silicate melts by thermal diffusion. *Nature*, *464*(7287), 396–400. https://doi.org/10.1038/nature08840

Huang, F., Chen, L., Wu, Z., & Wang, W. (2013). First-principles calculations of equilibrium Mg isotope fractionations between garnet, clinopyroxene, orthopyroxene, and olivine: Implications for Mg isotope thermometry. *Earth and Planetary Science Letters*, *367*, 61–70. https://doi.org/10.1016/j.epsl.2013.02.025

Huang, J., Huang, F., Wang, Z., Zhang, X., & Yu, H. (2017). Copper isotope fractionation during partial melting and melt percolation in the upper mantle: Evidence from massif peridotites in Ivrea-Verbano Zone, Italian Alps. *Geochimica et Cosmochimica Acta*, *211*, 48–63. https://doi.org/10.1016/j.gca.2017.05.007

Huang, J., Liu, S.-A., Wörner, G., Yu, H., & Xiao, Y. (2016). Copper isotope behavior during extreme magma differentiation and degassing: A case study on Laacher See Phonolite Tephra (East Eifel, Germany). *Contributions to Mineralogy and Petrology*, *171*, 1–16.

Huang, J., Xiao, Y. L., Gao, Y. J., Hou, Z. H., & Wu, W. P. (2012). Nb–Ta fractionation induced by fluid-rock interaction in subduction-zones: Constraints from UHP eclogite- and vein-hosted rutile from the Dabie orogen, central-eastern China. *Journal of Metamorphic Geology*, *30*(8), 821–842. https://doi.org/10.1111/j.1525-1314.2012.01000.x

Ionov, D. A., & Seitz, H.-M. (2008). Lithium abundances and isotopic compositions in mantle xenoliths from subduction and intra-plate settings: Mantle sources vs. eruption histories. *Earth and Planetary Science Letters*, *266*(3-4), 316–331. https://doi.org/10.1016/j.epsl.2007.11.020

Jenner, F. E., & O'Neill, H. S. C. (2012). Analysis of 60 elements in 616 ocean floor basaltic glasses. *Geochemistry, Geophysics, Geosystems*, *13*, Q02005. https://doi.org/10.1029/02011GC004009

Jochum, K. P., & Nohl, U. (2008). Reference materials in geochemistry and environmental research and the GeoReM database. *Chemical Geology*, *253*(1-2), 50–53. https://doi.org/10.1016/j.chemgeo.2008.04.002

Johnson, K. T. M., Dick, H. J. B., & Shimizu, N. (1990). Melting in the oceanic upper mantle: An ion microprobe study of diopsides in abyssal peridotites. *Journal of Geophysical Research*, *95*, 2661–2678.

Kang, J.-T., Ionov, D. A., Liu, F., Zhang, C.-L., Golovin, A. V., Qin, L.-P., et al. (2017). Calcium isotopic fractionation in mantle peridotites by melting and metasomatism and Ca isotope composition of the bulk silicate earth. *Earth and Planetary Science Letters*, *474*, 128–137. https://doi.org/10.1016/j.epsl.2017.05.035

Kelemen, P. B., Dick, H. J. B., & Quick, J. E. (1992). Formation of harzburgite by pervasive melt/rock reaction in the upper mantle. *Nature*, *358*(6388), 635–641. https://doi.org/10.1038/358635a0

Kelemen, P. B., Shimizu, N., & Salters, V. J. M. (1995). Extraction of mid-ocean-ridge basalt from the upwelling mantle by focused flow of melt in dunite channels. *Nature*, *375*(6534), 747–753. https://doi.org/10.1038/375747a0

Klein, E. M., & Langmuir, C. H. (1987). Global correlations of ocean ridge basalt chemistry with axial depth and crustal thickness. *Journal of Geophysical Research*, *92*(B8), 8089–8115. https://doi.org/10.1029/JB092iB08p08089

Lai, Y.-J., Pogge von Strandmann, P. A. E., Dohmen, R., Takazawa, E., & Elliott, T. (2015). The influence of melt infiltration on the Li and Mg isotopic composition of the Horoman Peridotite Massif. *Geochimica et Cosmochimica Acta*, *164*, 318–332. https://doi.org/10.1016/j.gca.2015.05.006

Le Grand, M., Ramos, A. Y., Calas, G., Galoisy, L., Ghaleb, D., & Pacaud, F. (2000). Zinc environment in aluminoborosilicate glasses by Zn K-edge extended X-ray absorption fine structure spectroscopy. *Journal of Materials Research*, *15*(09), 2015–2019. https://doi.org/10.1557/JMR.2000.0289

Le Roux, V., Lee, C. T. A., & Turner, S. J. (2010). Zn/Fe systematics in mafic and ultramafic systems: Implications for detecting major element heterogeneities in the Earth's mantle. *Geochimica et Cosmochimica Acta*, *74*(9), 2779–2796. https://doi.org/10.1016/j.gca.2010.02.004

Li, Y., & Audétat, A. (2012). Partitioning of V, Mn, Co, Ni, Cu, Zn, As, Mo, Ag, Sn, Sb, W, Au, Pb, and Bi between sulfide phases and hydrous basanite melt at upper mantle conditions. *Earth and Planetary Science Letters*, *355-356*, 327–340. https://doi.org/10.1016/j.epsl.2012.08.008

Li, S., Xiao, Y., Liu, D., Chen, Y., Ge, N., Zhang, Z., et al. (1993). Collision of the North China and Yangtze blocks and formation of coesite-bearing eclogites: timing and processes. *Chemical Geology*, *109*(1–4), 89–111. https://doi.org/10.1016/0009-2541(93)90063-O

Liu, S.-A., Huang, J., Liu, J., Wörner, G., Yang, W., Tang, Y.-J., et al. (2015). Copper isotopic composition of the silicate Earth. *Earth and Planetary Science Letters*, *427*, 95–103. https://doi.org/10.1016/j.epsl.2015.06.061

Liu, S.-A., Wang, Z.-Z., Li, S.-G., Huang, J., & Yang, W. (2016). Zinc isotope evidence for a large-scale carbonated mantle beneath eastern China. *Earth and Planetary Science Letters*, *444*, 169–178. https://doi.org/10.1016/j.epsl.2016.03.051

Lorand, J. P. (1989). Abundance and distribution of CuFeNi sulfides, sulfur, copper and platinum-group elements in orogenic-type spinel lherzolite massifs of Ariège (northeastern Pyrenees, France). *Earth and Planetary Science Letters*, *93*(1), 50–64. https://doi.org/10.1016/0012-821X(89)90183-0

Maréchal, C. N., Télouk, P., & Albarède, F. (1999). Precise analysis of copper and zinc isotopic compositions by plasma-source mass spectrometry. *Chemical Geology*, *156*(1–4), 251–273. https://doi.org/10.1016/S0009-2541(98)00191-0

Mazzucchelli, M., Rivalenti, G., Brunelli, D., Zanetti, A., & Boari, E. (2009). Formation of highly refractory dunite by focused percolation of pyroxenite-derived melt in the Balmuccia Peridotite Massif (Italy). *Journal of Petrology*, *50*(7), 1205–1233. https://doi.org/10.1093/petrology/egn053

Mazzucchelli, M., Zanetti, A., Rivalenti, G., Vannucci, R., Correia, C. T., & Tassinari, C. C. G. (2010). Age and geochemistry of mantle peridotites and diorite dykes from the Baldissero body: Insights into the Paleozoic-Mesozoic evolution of the Southern Alps. *Lithos*, *119*(3-4), 485–500. https://doi.org/10.1016/j.lithos.2010.08.002

McDonough, W. F. (2014). 3.16—Compositional model for the Earth's core A2—Holland, Heinrich D. In K. K. Turekian (Ed.), *Treatise on geochemistry* (2nd ed., pp. 559–576). Oxford: Elsevier. https://doi.org/10.1016/B978-0-08-095975-7.00215-1

Moeller, K., Schoenberg, R., Pedersen, R.-B., Weiss, D., & Dong, S. (2012). Calibration of the new certified reference materials ERM-AE633 and ERM-AE647 for copper and IRMM-3702 for zinc isotope amount ratio determinations. *Geostandards and Geoanalytical Research*, *36*(2), 177–199. https://doi.org/10.1111/j.1751-908X.2011.00153.x

Moynier, F., Paniello, R. C., Gounelle, M., Albarède, F., Beck, P., Podosek, F., & Zanda, B. (2011). Nature of volatile depletion and genetic relationships in enstatite chondrites and aubrites inferred from Zn isotopes. *Geochimica et Cosmochimica Acta*, *75*(1), 297–307. https://doi.org/10.1016/j.gca.2010.09.022

Moynier, F., Vance, D., Fujii, T., & Savage, P. (2017). The isotope geochemistry of zinc and copper. *Reviews in Mineralogy and Geochemistry*, *82*(1), 543–600. https://doi.org/10.2138/rmg.2017.82.13

Mukasa, S. B., & Shervais, J. W. (1999). Growth of subcontinental lithosphere: Evidence from repeated dike injections in the Balmuccia lherzolite massif, Italian Alps. *Lithos*, *48*(1-4), 287–316. https://doi.org/10.1016/S0024-4937(99)00033-X

Niu, Y. L. (1997). Mantle melting and melt extraction processes beneath ocean ridges: Evidence from abyssal peridotites. *Journal of Petrology*, *38*(8), 1047–1074. https://doi.org/10.1093/petroj/38.8.1047

Niu, Y. L., & Hekinian, R. (1997). Basaltic liquids and harzburgitic residues in the Garrett transform: A case study at fast-spreading ridges. *Earth and Planetary Science Letters*, *146*(1-2), 243–258. https://doi.org/10.1016/S0012-821X(96)00218-X

Obermiller, W. A. (1994). Chemical and isotopic variations in the Balmuccia, Baldissero and Finero Peridotite Massifs (Ivrea-Zone, Italy), (PhD thesis, p. 191) Johannes Gutenberg-Universitat Mainz.

Oeser, M., Dohmen, R., Horn, I., Schuth, S., & Weyer, S. (2015). Processes and time scales of magmatic evolution as revealed by Fe-Mg chemical and isotopic zoning in natural olivines. *Geochimica et Cosmochimica Acta*, *154*, 130–150. https://doi.org/10.1016/j.gca.2015.01.025

O'Reilly, S. Y., Griffin, W. L., & Ryan, C. G. (1991). Residence of trace elements in metasomatized spinel lherzolite xenoliths: a proton-microprobe study. *Contributions to Mineralogy and Petrology*, *109*(1), 98–113. https://doi.org/10.1007/BF00687203

Palme, H., & O'Neill, H. S. C. (2014). 3.1—Cosmochemical estimates of mantle composition A2—Holland, Heinrich D. In K. K. Turekian (Ed.), *Treatise on geochemistry* (2nd ed., pp. 1–39). Oxford: Elsevier. https://doi.org/10.1016/B978-0-08-095975-7.00201-1

Peressini, G., Quick, J. E., Sinigoi, S., Hofmann, A. W., & Fanning, M. (2007). Duration of a large mafic intrusion and heat transfer in the lower crust: A SHRIMP U-Pb zircon study in the Ivrea-Verbano Zone (western Alps, Italy). *Journal of Petrology*, *48*(6), 1185–1218. https://doi.org/10.1093/petrology/egm014

Petit, J. C. J., de Jong, J., Chou, L., & Mattielli, N. (2008). Development of Cu and Zn isotope MC-ICP-MS measurements: Application to suspended particulate matter and sediments from the Scheldt estuary. *Geostandards and Geoanalytical Research*, *32*(2), 149–166. https://doi.org/10.1111/j.1751-908X.2008.00867.x

Pichat, S., Douchet, C., & Albarède, F. (2003). Zinc isotope variations in deep-sea carbonates from the eastern equatorial Pacific over the last 175 ka. *Earth and Planetary Science Letters*, *210*(1-2), 167–178. https://doi.org/10.1016/S0012-821X(03)00106-7

Pogge von Strandmann, P. A. E., Elliott, T., Marschall, H. R., Coath, C., Lai, Y.-J., Jeffcoate, A. B., & Ionov, D. A. (2011). Variations of Li and Mg isotope ratios in bulk chondrites and mantle xenoliths. *Geochimica et Cosmochimica Acta*, *75*(18), 5247–5268. https://doi.org/10.1016/j.gca.2011.06.026

Pons, M.-L., Debret, B., Bouilhol, P., Delacour, A., & Williams, H. (2016). Zinc isotope evidence for sulfate-rich fluid transfer across subduction zones. *Nature Communications*, *7*, 13794. https://doi.org/10.1038/ncomms13794

Richter, F. M., Davis, A. M., DePaolo, D. J., & Watson, E. B. (2003). Isotope fractionation by chemical diffusion between molten basalt and rhyolite. *Geochimica et Cosmochimica Acta*, *67*(20), 3905–3923. https://doi.org/10.1016/S0016-7037(03)00174-1

Rivalenti, G., Mazzucchelli, M., Vannucci, R., Hofmann, A. W., Ottolini, L., Bottazzi, P., & Obermiller, W. (1995). The relationship between websterite and peridotite in the Balmuccia peridotite massif (NW Italy) as revealed by trace element variations in clinopyroxene. *Contributions to Mineralogy and Petrology*, *121*(3), 275–288. https://doi.org/10.1007/BF02688243

Rudnick, R. L., & Ionov, D. A. (2007). Lithium elemental and isotopic disequilibrium in minerals from peridotite xenoliths from far-east Russia: Product of recent melt/fluid-rock reaction. *Earth and Planetary Science Letters*, *256*(1-2), 278–293. https://doi.org/10.1016/j.epsl.2007.01.035

Salters, V. J. M., & Stracke, A. (2004). Composition of the depleted mantle. *Geochemistry, Geophysics, Geosystems*, *5*, Q05B07. https://doi.org/10.1029/2003GC000597

Savage, P. S., Moynier, F., Chen, H., Shofner, G., Siebert, J., Badro, J., & Puchtel, I. S. (2015). Copper isotope evidence for large-scale sulphide fractionation during Earth's differentiation. *Geochemical Perspectives Letters*, *1*, 53–64.

Schauble, E. A. (2004). Applying stable isotope fractionation theory to new systems. *Reviews in Mineralogy and Geochemistry*, *55*(1), 65–111. https://doi.org/10.2138/gsrmg.55.1.65

Shannon, R. D. (1976). Revised effective ionic radii and systematic studies of interatomic distances in halides and chalcogenides. *Acta Crystallographica*, *32*(5), 751–767. https://doi.org/10.1107/S0567739476001551

Shervais, J. W., & Mukasa, S. B. (1991). The Balmuccia orogenic lherzolite massif, Italy. *Journal of Petrology*, *Special_Volume*(2), 155–174. https://doi.org/10.1093/petrology/Special_Volume.2.155

Sinigoi, S., Cominchiaramonti, P., Demarchi, G., & Siena, F. (1983). Differentiation of partial melts in the mantle: Evidence from the Balmuccia peridotite, Italy. *Contributions to Mineralogy and Petrology*, *82*(4), 351–359. https://doi.org/10.1007/BF00399712

Sio, C. K. I., Dauphas, N., Teng, F.-Z., Chaussidon, M., Helz, R. T., & Roskosz, M. (2013). Discerning crystal growth from diffusion profiles in zoned olivine by in-situ Mg-Fe isotopic analyses. *Geochimica et Cosmochimica Acta*, *123*, 302–321. https://doi.org/10.1016/j.gca.2013.06.008

Sossi, P. A., Halverson, G. P., Nebel, O., & Eggins, S. M. (2015). Combined separation of Cu, Fe and Zn from rock matrices and improved analytical protocols for stable isotope determination. *Geostandards and Geoanalytical Research*, *39*(2), 129–149. https://doi.org/10.1111/j.1751-908X.2014.00298.x

Sossi, P. A., Nebel, O., & Foden, J. (2016). Iron isotope systematics in planetary reservoirs. *Earth and Planetary Science Letters*, *452*, 295–308. https://doi.org/10.1016/j.epsl.2016.07.032

Sossi, P. A., Nebel, O., O'Neill, H. S. C., & Moynier, F. (2018). Zinc isotope composition of the Earth and its behaviour during planetary accretion. *Chemical Geology*, *471*, 125–135.

Spandler, C., & O'Neill, H. S. C. (2010). Diffusion and partition coefficients of minor and trace elements in San Carlos olivine at 1,300°C with some geochemical implications. *Contributions to Mineralogy and Petrology*, *159*(6), 791–818. https://doi.org/10.1007/s00410-009-0456-8

Telus, M., Dauphas, N., Moynier, F., Tissot, F. L. H., Teng, F.-Z., Nabelek, P. I., et al. (2012). Iron, zinc, magnesium and uranium isotopic fractionation during continental crust differentiation: The tale from migmatites, granitoids, and pegmatites. *Geochimica et Cosmochimica Acta*, *97*, 247–265. https://doi.org/10.1016/j.gca.2012.08.024

Teng, F.-Z., Dauphas, N., Helz, R. T., Gao, S., & Huang, S. (2011). Diffusion-driven magnesium and iron isotope fractionation in Hawaiian olivine. *Earth and Planetary Science Letters*, *308*(3-4), 317–324. https://doi.org/10.1016/j.epsl.2011.06.003

Walter, M. J. (1998). Melting of garnet peridotite and the origin of komatiite and depleted lithosphere. *Journal of Petrology*, *39*(1), 29–60. https://doi.org/10.1093/petroj/39.1.29

Wang, Z.-C., & Becker, H. (2013). Ratios of S, Se and Te in the silicate earth require a volatile-rich late veneer. *Nature*, *499*(7458), 328–331. https://doi.org/10.1038/nature12285

Wang, Z.-C., & Becker, H. (2015a). Fractionation of highly siderophile and chalcogen elements during magma transport in the mantle: Constraints from pyroxenites of the Balmuccia peridotite massif. *Geochimica et Cosmochimica Acta*, *159*, 244–263. https://doi.org/10.1016/j.gca.2015.03.036

Wang, Z.-C., & Becker, H. (2015b). Abundances of Ag and Cu in mantle peridotites and the implications for the behavior of chalcophile elements in the mantle. *Geochimica et Cosmochimica Acta*, *160*, 209–226. https://doi.org/10.1016/j.gca.2015.04.006

Wang, Z.-C., Becker, H., & Gawronski, T. (2013). Partial re-equilibration of highly siderophile elements and the chalcogens in the mantle: A case study on the Baldissero and Balmuccia peridotite massifs (Ivrea Zone, Italian Alps). *Geochimica et Cosmochimica Acta*, *108*, 21–44. https://doi.org/10.1016/j.gca.2013.01.021

Wang, Z.-Z., Liu, S.-A., Liu, J., Huang, J., Xiao, Y., Chu, Z.-Y., et al. (2017). Zinc isotope fractionation during mantle melting and constraints on the Zn isotope composition of Earth's upper mantle. *Geochimica et Cosmochimica Acta*, *198*, 151–167. https://doi.org/10.1016/j.gca.2016.11.014

Weyer, S., & Ionov, D. A. (2007). Partial melting and melt percolation in the mantle: The message from Fe isotopes. *Earth and Planetary Science Letters*, *259*(1-2), 119–133. https://doi.org/10.1016/j.epsl.2007.04.033

Zhao, X.-M., Zhang, Z., Huang, S., Liu, Y., Li, X., & Zhang, H. (2017). Coupled extremely light Ca and Fe isotopes in peridotites. *Geochimica et Cosmochimica Acta*, *208*, 368–380. https://doi.org/10.1016/j.gca.2017.03.024

Zheng, J. P., Sun, M., Griffin, W. L., Zhou, M. F., Zhao, G. C., Robinson, P., et al. (2008). Age and geochemistry of contrasting peridotite types in the Dabie UHP belt, eastern China: Petrogenetic and geodynamic implications. *Chemical Geology*, *247*(1–2), 282–304. https://doi.org/10.1016/j.chemgeo.2007.10.023